UNIVERSITY OF LEEDS

This is a repository copy of *Concentration profiling of a horizontal sedimentation tank utilising a bespoke acoustic backscatter array and CFD simulations*.

White Rose Research Online URL for this paper:
http://eprints.whiterose.ac.uk/156883/

Version: Accepted Version

Article:
Hunter, TN orcid.org/0000-0003-3922-491X, Peakall, J orcid.org/0000-0003-3382-4578, Egarr, D et al. (12 more authors) (2020) Concentration profiling of a horizontal sedimentation tank utilising a bespoke acoustic backscatter array and CFD simulations. Chemical Engineering Science, 218. 115560. ISSN 0009-2509

https://doi.org/10.1016/j.ces.2020.115560

© 2020, Elsevier. This manuscript version is made available under the CC-BY-NC-ND 4.0 license http://creativecommons.org/licenses/by-nc-nd/4.0/.

Reuse
This article is distributed under the terms of the Creative Commons Attribution-NonCommercial-NoDerivs (CC BY-NC-ND) licence. This licence only allows you to download this work and share it with others as long as you credit the authors, but you can't change the article in any way or use it commercially. More information and the full terms of the licence here: https://creativecommons.org/licenses/

Takedown
If you consider content in White Rose Research Online to be in breach of UK law, please notify us by emailing eprints@whiterose.ac.uk including the URL of the record and the reason for the withdrawal request.

White Rose university consortium
Universities of Leeds, Sheffield & York

eprints@whiterose.ac.uk
https://eprints.whiterose.ac.uk/

Concentration profiling of a horizontal sedimentation tank utilising a bespoke acoustic backscatter array and CFD simulations

Timothy N. Hunter[a], Jeff Peakall[b], Darrell Egarr[c, 1], David M.J. Cowell[d], Steven Freear[d], Alastair S. Tonge[a], Lucy Horton[c, 1], Hugh P. Rice[a], Iain Smith[a], Kevin Malone[c, 2], David Burt[e], Martyn Barnes[f], Geoff Randall[f], Simon Biggs[g], Michael Fairweather[a]

[a] School of Chemical and Process Engineering, University of Leeds, Leeds LS2 9JT, U.K.

[b] School of Earth and Environment, University of Leeds, Leeds LS2 9JT, U.K.

[c] MMI Engineering Ltd. Unit 2, Corum Office Park, Crown Way, Bristol BS30 8FJ, U.K.

[d] School of Electronic and Electrical Engineering, University of Leeds, Leeds LS2 9JT, U.K.

[e] Department of Mechanical Engineering, University of Bristol, Bristol BS8 1TR, U.K.

[f] Sellafield Ltd. Hinton House, Birchwood Park Ave, Warrington WA3 6GR, U.K.

[g] The University of Western Australia, Perth, WA 6009, Australia

[1]current address: Dyson Ltd., Tetbury Hill, Wiltshire SN16 0RP, U.K

[2]current address: Urenco Nuclear Stewardship Ltd. Capenhurst Ln, Capenhurst, Chester CH1 6ER, U.K.

Abstract

The performance of a pilot-scale horizontal sedimentation tank was characterised utilising computational fluid dynamics (CFD) and a bespoke ultrasonic backscatter array, for both spherical glass and flocculated calcite separation. The CFD simulation was developed in OpenFOAM, using algebraic slip and hindered settling models, in order to solve the transport of multiple particle size classes, enabled through a population balance approach. Simulations of concentration compared closely to samples for the glass dispersions, but under-predicted concentration with flocculated calcite (likely due to complexities from modelling floc break-up in the mixer). In comparison, the acoustic array measured the calcite concentration with a high degree of resolution, where in particular, evidence suspension mobilisation near the outlet was observed, due to recirculation. Overall, we demonstrate the performance and current limitations of large-scale CFD for complex floc systems, as well as the use of ultrasonics to significantly aid process understanding, through online monitoring of solid-liquid separations.

Keywords:

Acoustic backscatter systems; ultrasonics; CFD; horizontal sedimentation; clarifier; flocculation.

1 Introduction

The characterisation of large-scale solid-liquid separators is critically important for a range of industries; from water and wastewater treatment to minerals processing and paper production e.g. (Benn et al., 2018; Ramin et al., 2014; Zhang et al., 2015a). Understanding separation changes with variations in feed composition or flow regimes are key concerns, which can lead to significant downstream issues if performance is reduced. However, due to the complex nature of both the fluid dynamics and particle phase (which are often present as shear dependent fractal aggregates) it is extremely difficult to extrapolate fundamental measureable properties, such as sampled aggregate sizes or batch sedimentation rates, to industrial separation performance (Concha et al., 2017; Karpinska and Bridgeman, 2016).

Such operational issues have led to a large body of work focused on modelling (both analytical and numerical) and hydrodynamic simulation of large-scale operations, including work on primary horizontal or radial settlers, commonly known as clarifiers (Asgharzadeh et al., 2011; Fan et al., 2007; Goula et al., 2008; Shahrokhi et al., 2012; Stamou et al., 1989) and secondary thickeners (Gladman et al., 2010; Guyonvarch et al., 2015; Zhang et al., 2015a). Aspects such as feedwell design and the effect of baffles on turbulence and recirculation have been particular areas of attention e.g. (Asgharzadeh et al., 2011; Burt, 2010; Das et al., 2016; Farrow et al., 2000; Guo et al., 2017; Razmi et al., 2013; Salem et al., 2011; Tarpagkou and Pantokratoras, 2014). While many of these studies were able to simulate single phase flows in complex geometries with a high degree of accuracy, fully incorporating the particle physics remains a significant challenge, due to their complex structure and shear-dependent aggregation kinetics (Karpinska and Bridgeman, 2016). Additionally, large-scale simulations often lack high-quality experimental data to enable adequate model validation.

Although simulating the sedimentation of spherical particles across a wide concentration range can be quantitatively achieved using mixture viscosity models with high degrees of accuracy (Antonopoulou et al., 2018), the interaction of more common complex agglomerates (in both low concentration suspensions and consolidated thickener zones) is often undertaken using more empirically based approaches (Bridgeman et al., 2010; Gladman et al., 2010; Johnson et al., 2016; Torfs et al., 2017; Zhang et al., 2015b). Recent work has highlighted improvements in sedimentation dynamics and incorporation into computational fluid dynamic simulations by utilising sludge rheology (Ramin et al., 2014) or improved force-based mechanistic models (Xu et al., 2017) although translation to flow systems is predicated on sampled sludge properties being consistent in the operational units. Indeed, in many settlers, sludge properties will vary through the

process, where issues of turbulence induced flocculation and aggregate breakup are particularly important and difficult phenomena to account for. For example, previous studies have investigated the role of polymeric flocculant type, dose and mixing on floc size or structure (Costine et al., 2018) and the modelling of this behaviour using population balance approaches (Jeldres et al., 2018; Peña et al., 2017; Vajihinejad and Soares, 2018). Whilst such work highlights the progress in modelling complex particle properties, these have largely not been fully integrated into full-scale studies of solid-liquid separators to date.

Consequently, there is a need for improved simulations of solid-liquid separators, and in particular, a requirement for high quality experimental data from large-scale operations e.g., of particle concentration changes through the separator, to aid improvement and validation of these models. Furthermore, development of online or *in situ* measurement techniques that reduce time consuming sampling would have further advantages, giving the potential of real-time process monitoring and control. Nevertheless, although there has been great progress in the use of chemical sensors (Vanrolleghem and Lee, 2003), experimental techniques that allow continuous, on-line monitoring of large-scale solid-liquid separators that avoid the hazards and large physical footprint of x-ray or gamma-ray instruments (Benn et al., 2018; De Clercq et al., 2005) have remained fairly limited (Concha et al., 2017).

For flow characteristics, *in situ* measurements can be achieved through techniques such as Doppler profilers (Mohanarangam et al., 2013; Tarud et al., 2010; Vanrolleghem et al., 2006). In terms of particle property measurement, while image analysers (Concha et al., 2017; Derlon et al., 2017) and focused beam reflectance monitors (De Clercq et al., 2004; Farrow et al., 2000) have been utilised to measure particle size or shape, characterising the settling dynamics within sludge settling zones is generally achieved only through interfacial sludge blanket monitors (Schewerda et al., 2013). Electromagnetic attenuation, such as gamma-ray systems, have been used to profile sediment concentrations in large-scale separators (Benn et al., 2018; Jaworski and Meng, 2009), however such techniques have high cost and logistical difficulties for wide scale adoption on plants. As an alternative, acoustic backscatter systems (ABS) offer a potential technique that is able to measure a number of particle properties *in situ*, with the flexibility and low cost to be applicable to real industrial operations (Hunter et al., 2012a; Stener et al., 2016; Thorne and Hurther, 2014). While such systems are normally applied for environmental monitoring applications (Guerrero et al., 2016; Thorne and Hanes, 2002; Wilson and Hay, 2015) they have previously been used by the current authors to track suspension sedimentation in laboratory columns (Bux et al., 2015; Hunter

et al., 2012b) larger scale liquid-jet mixers (Bux et al., 2017) and slurry flow in pipes (Rice et al., 2014; Rice et al., 2015).

Despite the potential of ABS from previous research, the use of this technique for full-scale monitoring represents a significant challenge, requiring both the development of new instrumentation capable of high fidelity multipoint profiling, and enhanced knowledge of the acoustical response of relevant aggregated suspensions. Therefore, to gain greater insight into the use these systems for industrial deployment, this paper presents the application of a newly designed ultrasonic backscatter instrument and transducer array for concentration profiling in a large-scale horizontal sedimentation tank. The clarifier described is representative of a nuclear waste transfer operation, where there is an acute need for remote real-time monitoring, without the requirement for any physical site exposure (due to the radiological hazards). Additionally, in order to understand the capability of simulations to predict the settling performance of complex flocculated wastes, a CFD model of the same system is also developed, using open source code and a population balance approach, which is compared and validated against acoustics and sampled concentration data. Critically, the model includes an innovative approach to incorporating flocculation and aggregate breakage kinetics, developed from previous work by Heath *et al.* (2006b). Studies were conducted with both well dispersed glass and flocculated calcite suspensions, to investigate the effect of shear-dependent aggregation on settling and flow dynamics, and the resulting influence on predicted separation behaviour. Different methods of acoustic backscatter analysis were also employed to determine the best approach for the concentration changes encountered.

2 Experimental

2.1 Materials

Two particle types were tested in the clarifier trials. Initially, relatively monodisperse and spherical glass powder 'Honite-22' (Guyson International, U.K) with a nominal D_{50} of ~44 μm was used as a model baseline system. Flocculated calcium carbonate (calcite) was also used as a representative minerals waste suspension, while it is structurally characteristic of corroded nuclear cladding wastes (Bux et al., 2015, Johnson et al., 2016). The calcite utilised was 'Omyacarb 2' (Omya, U.K) with a nominal D_{50} of ~6 μm. The particle size distributions for the two dispersion types are shown in Fig. 1. The calcite particles were flocculated with a high molecular weight, medium charge density anionic polymer 'Flowpam AN934SH' (SNF Ltd., U.K). Similar flocculated calcite systems have been investigated in studies of model mineral solid-liquid separations (Benn et al.,

2018; Gladman et al., 2010; Heath et al., 2006a; Hunter et al., 2015; Spehar et al., 2015; van Deventer et al., 2011).

2.2 Optimisation of polymer floc dose

To optimise the polymer dose for calcite floc formation in the clarifier trials, pre-trial experiments were conducted in a 30 l baffled column mixer with a 7.6 cm (3 inch) axial impeller set to 380 rpm (to replicate a medium shear environment). A 4 wt% suspension of calcite was pre-mixed for 15 minutes. Then, a 1000 ppm stock solution of the polymer was added dropwise to give final concentrations of 1 – 100 ppm_v (volume base) in the mixer. For each trial, a D600V (Metler-Toledo) Focused Beam Reflectance Monitor (FBRM) was inserted into the top 1/3 of the mixer and particle chord lengths recorded. Fig. 2 (a) shows the measured median chord length over time for polymer additions of 1, 6 and 40 ppm.

Additionally, flocculated calcite suspensions (mixed for 5 minutes using the same conditions as above) were separated into 500 ml settling cylinders, and average settling rates measured for polymer dosages of 1 – 100 ppm. Resultant settling rates versus polymer dose are shown in Fig. 2 (b). Both FBRM and settling measurements suggest an optimal polymer concentration of around 40 ppm, as this concentration led to large measured particle sizes and the fastest sedimentation rates. This level is consistent with a previous study on the same polymer-particle system in a pilot scale vertical thickener (Hunter et al., 2015) and FBRM measurements in a pipe-flocculator (Heath et al., 2006a). However, such dosages were deemed potentially problematic for the clarifier work, due to the large total amount required for all trials. Hence, a pragmatic polymer dose of 10 ppm was selected, as it gave adequate flocculation and settling performance for requirements.

2.3 Design and operational setup of the horizontal clarifier

The large-scale trials were conducted at NSG Environmental in Chorley, UK. A bespoke 9 m^3 clarifier was built, 4.86 m in length, 2.46 m liquid depth and 0.75 m wide. The design was an approximate 1/3 scale model of a settling tank employed by the UK nuclear industry as a waste separator; although, it is nominally similar to horizontal- flow clarifiers used throughout front-end water treatment and minerals processing operations (albeit with a shortened length to width ratio) (Asgharzadeh et al., 2011; Egarr et al., 2016; Fan et al., 2007; Razmi et al., 2013). The clarifier incorporated an initial baffled section, from the inlet to 0.5 m length, creating a separate mixing zone. A 0.2 m diameter axial impeller (running at moderate shear of 300 rpm) was inserted ~1 m deep into the baffled mixing zone, so that the blade was close to the tank inlet point. As no inlet distributer was used, this arrangement was intended to ensure relatively homogenous mixing of the

test suspensions (either the non-flocculated glass or flocculated calcite). A 0.3 m deep weir allowed suspensions to propagate from the mixing zone into the settling section of the clarifier (being the remaining ~4.3 m in length). The outlet weir was a 0.05 × 0.3 m^2 section cut into the back side of the clarifier. A schematic of the clarifier is displayed in Fig. 3 (a).

Three large feed tanks (also of 9 m^3) of homogenously mixed testing suspensions at ~ 34 g/l, were connected with a monopump and a 2.5 cm line to the inlet of the mixer-settler tank. The feed rate was set at 80 l/min, which approximately allowed for 3 tank volumes to be exchanged over a testing period of 4.5 hours (the settling tank was initially filled with mains water). A line injection port was positioned 5.3 m from the tank inlet, where polymer was introduced from a 2000 ppm stock (using a small peristaltic pump) at such a rate to give a diluted feed concentration of 10 ppm. It was assumed that the 5 metre lead-in section would be sufficient to allow for high levels of flocculation without over-shearing, which may secondarily reduce aggregate size. This understanding was based on previous work by Heath and co-workers, looking at flocculation in a 2.5 cm pipe-reactor using the same polymer-particle system (Heath et al., 2006a).

2.4 Clarifier settling trials and integration of the acoustic backscatter array

Five evenly spaced horizontal locations along the settling section of the clarifier were chosen for measuring particle concentration, all at 0.705 m intervals from the inlet to the settling section (length positions (i) – (v), as shown in Fig. 3 (a)). Sampled extractions were made at five vertical points using a multi-head peristaltic pump, at heights of 27, 47, 67, 107 and 177 cm from the tank base (depth points 7, 6, 5, 3 and 1 respectively, as shown in Fig. 3 (a)). The sampling pole was off-set from the central plane of the clarifier by 7.5 cm.

Concentration sampling data were coupled with data from an acoustic backscatter system (ABS). The instrument utilised in the clarifier trials was a bespoke device designed and developed at the School of Electronic and Electrical Engineering, University of Leeds, known as the Ultrasonic Array Research Platform (UARP) Mark 2. Details of the device have been presented in a previous publication (Cowell et al., 2015) with descriptions of the related underlying architecture also reported (Cowell et al., 2013; Smith et al., 2012). The controller was connected to a vertical array of seven immersion transducers of 2.25 MHz central frequency and 0.25 inch active element diameter (Olympus NDT V323) via an 8 metre RG174 coaxial cable of 50 Ω characteristic impedance. The probes were positioned at 20^o to vertically downwards, so that it was possible to measure a close-to-vertical profile distance without interference from each other. During

measurement sequences, excitation was performed at frequencies of 2.0, 2.25 and 2.5 MHz using 5 μs Hann windowed tone bursts (to reduce side lobe leakage (Zhang et al., 2019)) and the return pulse voltage was measured to a maximum depth of 300 mm. In total, 10,000 received waveforms were collected for each excitation setting and stored for post-processing (equating to ~ 3 minutes of acquisition time per measurement).

Five of the seven transducers were aligned with sample points. These probes were positioned at actual heights of 32, 52, 72, 112 and 182 cm from the tank base. The reason for the discrepancy in exact position was that the first 5 cm of acoustic data was normally discarded in analysis, due to near field interference (Rice et al., 2014) and thus, sample points corresponded to the upper analysis section of acoustic data. The additional probes were positioned at 92 and 147 cm from the tank base (depth points 4 and 2, respectively, as indicated in Fig. 3) giving extended measurements in the upper levels of the clarifier. The acoustic array was off-set by +7.5 cm from the clarifier central plane to minimise any interference from the sample pole. While the sample pole and acoustic array were thus not strictly co-located, it was assumed that any differences in lateral concentration were minimal. In addition to sampling and acoustic data, an FBRM probe was mounted into the mixing section of the clarifier, to gain *in situ* particle size measurements over the course of each trial. An image showing the settling tank with acoustic array and sampling pole, along with the mounted FBRM probe in the mixing zone, is shown in Fig 3 (b).

For each trial, the feed pump was opened (along with the polymer injection port for calcite studies) and the clarifier left to run initially for 30 minutes at the operating flow rate of 80 l/min. Then, sampling and acoustic data were taken first from length position (i), whereupon the array and sample pole were moved to location (ii) and the process repeated until position (v). After concentration sampling was complete at this initial time, it was repeated for four additional times, at intervals of 50 minutes (so measurement times of +30, +80, +130, +180 and +230 min from the start of the trial). In addition, samples of the feed (taken just before the tank inlet) and weir concentrations were taken at each time interval to characterise bulk separator performance. It is noted that due to the time taken to gain representative acoustic measurements at each location, measurements took ~20 minutes in total for each time across the five length positions. Therefore, small time lag exists in concentrations measured from one length position to another. For clarity, the initial time at each measurement interval is quoted only.

2.5 Computational fluid dynamics model of suspension separation within the clarifier

A population balance solver was developed using the open source code OpenFOAM v2.2.x. The model geometry was generated using ANSYS Design Modeler and the computational mesh using ANSYS ICEM. A structured two-dimensional hexahedral mesh was applied to the clarifier geometry (along the central plane) with approximately 14,000 elements, and is shown in the Electronic Supplementary Material (ESM), Fig. S1, giving an average cell size of ~900 mm^2 (which was reduced at the bottom and end walls). The resolution of the grid was based on previous experience of CFD modelling of settler design, at similar length and time scales, where grid independence studies were performed (Burt, 2010), suggesting the model resolution is sufficient. While the grid size was reduced towards the walls, the influence of wall effects explicitly were not considered significant. The reason was that the main focus of the study was to resolve the flow and concentrations within the bulk fluid around the measurement locations (all at distances > 0.2 m from the tank base and > 0.5 m from the end walls). Also, as the 2D central plane was 0.375 m from the side walls, it was assumed they would also not impact considerably on behaviour. The relaxation time used for dynamic equilibrium was estimated based on the time for a stationary particle to reach the terminal velocity under the force of gravity. For all apart from the very the largest particle size class modelled, this distance was < 2 mm, which was assumed to be sufficiently small with respects to the average computational cell size.

In all cases, clarifier inlet velocities were set to 2.63 m/s, in order to achieve the given flow rate of 80 l/min, while turbulence kinetic energy and dissipation rate were set to correspond to a turbulence intensity of 5%. For turbulence, the k-ε model was used (Jones and Launder, 1972), while the algebraic slip model was used to simulate the multiphase aspects of the flow. To calculate the additional thrust imparted into the flow from the impeller, implicitly, a CFD model was generated using ANSYS CFX R16.1. The impeller geometry was approximated using geometric length data from the actual impeller (with comparison shown in ESM, Fig. S2). The mechanical power from the impeller was calculated to be 54 W (using the standard power number equation (Crittenden et al., 2012)). A simulation was performed with the modelled 3D impeller geometry, which gave a thrust of 30.6 N, for an input power of 54 W, where the simulated impeller rpm for this power was within 10% of the measured rate. Liquid phase density and viscosity was set to be that of water at 16 ºC, while bulk fluid density was set with an initial particle concentration of 34 g/l (equating to experimental conditions). Both the multiphase bulk fluid density and viscosity were allowed to vary with particle concentration during the simulation, where fluid viscosity changes were approximated using the model of Bokil and Bewtra (1973), as also given in Das et al. (2016).

Overall for each run, the calculation time for the simulations was approximately 24 hours, using parallel processing across four cores.

For the spherical glass trials, the distribution shown in Fig. 1 was discretised into 10 size groups, with density set to that of glass (2450 kg/m^3). Sedimentation was incorporated through a Richardson-Zaki hindered settling model, to calculate particle terminal slip velocities (Brown and Lawler, 2003), similar to that recently described in the numerical simulation of settling silica spheres (Antonopoulou et al., 2018). Because this simple hindered settling model does not contain any limitation on maximum packing fraction, the settling model was extended to the consolidated bed at a maximum fraction equal to the loose packed sphere limit (~0.64 (Antonopoulou et al., 2018)). Any glass that settled within the settling zone were removed from the model at the same rate as settlement. This simplification was considered reasonable, as the glass beads formed a very thin bed which would not interact with the flow within the clarifier. Therefore, particle re-suspension from the bed was not integrated into the simulation, although, given the low turbulence prevalent at the base of the clarifier, no resuspension was expected.

For the flocculated calcite trials, a population balance approach was used, following the methodology of Biggs and Lant (2002) and as described by the current authors in previous publications (Burt, 2010; Egarr et al., 2016). To define the size groups, an initial primary solid particle diameter of 5.92 μm was used (correlating to the measured D_{50}) with the density of calcite (2710 kg/m^3). The growth and decay of aggregate sizes were incorporated into simulations by modification of the gPROMS population balance model of Heath *et al.* (2006b) who also directly measured the flocculation of the same calcite-polymer system in a similar pipe-flocculator. For the current study, the same equations were implemented into a Perl script, except that here the floc diameter rather than a mass effective diameter was used, with an assumed fractal dimension of 2.5 (Kim and Kramer, 2006) where for a constant fractal dimension, the density of the flocs will reduce with increase in size (Johnson et al., 2016). The population balance model used 20 particle size groups, and the results were verified against both the original gPROMS code and related experimental data, for flow conditions with a mean shear velocity gradient of 242 s^{-1}. These comparisons, showing average aggregate size versus time under the constant shear conditions, are given in the ESM, Fig. S3, and indicate a very good fit to the data. It is noted that given the distance from the polymer injection point to the clarifier, the expectation would be that aggregates will approach a maximum size of ~120 μm at the clarifier inlet (Heath et al., 2006a).

To include the effect of calcite flocculation on sedimentation, the hindered settling model was modified to incorporate the effective volume fraction of the overall aggregates and their associated density reduction, as considered originally by Michaels and Bolger (1962) and more recently described in relation to the sedimentation of coagulated mineral wastes (Johnson et al., 2016). One Additional limitation when modelling the transport of particulates using hindered settling functions in an Eulerian frame, is that the CFD solver does not explicitly consider a maximum particle packing order, and it is possible for the volume fraction of the solids phase to approach 1, unless a modification is implemented to prevent unphysical concentrations of the solid phase (Antonopoulou et al., 2018). Therefore, the settling model was extended in an attempt to bound the maximum volume fraction of the solids. A maximum packing fraction of 0.3 was estimated for the flocculated calcite based on measured concentrations within the bed, which is similar to outlet concentrations taken previously for the same suspension in a laboratory-scale thickener (Hunter et al., 2015). To achieve a stable bed concentration of this value, the hindered settling function was modified to reduce velocities towards zero at the maximum bed fraction. Additionally, two negative particle slip velocity equations were set for any conditions that went beyond the desired packing fraction to prevent discontinuities in the settling equations and to force the bed to self-balance. Given in Equations 1 – 3 are the modified hindered settling functions utilised in the simulation. Here, Φ is the volume fraction of the porous flocs, Φ_{max} is the maximum bed fraction (0.3), v_s is the estimated settling velocity and v_o is the velocity at zero particle concentration (estimated from the Stokes equation, using the calculated density of the flocs, rather than the specific particle density). Additionally, the exponent '*n*' was set at 4.65, as normal in low shear conditions (Johnson et al., 2016).

$$\text{If } \Phi < \Phi_{max} \qquad v_s = v_0(1-\Phi)^n\left(\frac{\Phi}{\Phi_{max}}\right) \tag{1}$$

$$\text{If } \Phi_{max} \leq \Phi < 2\Phi_{max} \qquad v_s = -v_0(1-\Phi')^n\left(\frac{\Phi'}{\Phi_{max}}\right) \tag{2}$$

$$\text{Where } \Phi' = 2\Phi_{max} - \Phi$$

$$\text{If } \Phi > 2\Phi_{max} \qquad v_s = -4v_0 \tag{3}$$

The limitation of this approach is that the solids concentration within the bed itself becomes a constant value at the set maximum packing fraction. Therefore, it was not possible to model the graduated increase in concentration that normally occurs in bed consolidation (Benn et al., 2018). However, attempting to more accurately model bed fraction was considered out of the scope of the

simulation, as the focus was to understand changes in concentration within the bulk sedimentation zone in the clarifier, and the potential impact on solid levels in the downstream outlet.

3 Results and Discussion

3.1 Comparison between experimental sampling and CFD predictions of concentration with spherical glass

Averaged values of the feed and weir samples for the spherical glass dispersion trial at the five measurement times are shown within the ESM (Fig. S4 (a) and (b)). Feed samples were relatively constant across the total trial, with some small variation, likely a result of changeover between feed tanks. The weir samples showed slightly larger variation, attributed to the build-up of particles in the clarifier over time (as it was originally filled purely with water) and gave an average value of ~0.75 g/l (or ~301 ppm_v), which is above those expected for good clarifier performance (Razmi et al., 2013; Stamou et al., 1989; Tarpagkou and Pantokratoras, 2014) indicating the system was not optimised for the spherical glass. However, it is noted that the flowrate used in the clarifier (80 l/min) was determined from settling rates for the flocculated calcite (see Fig. 2 (a)) and it can be reasonably assumed (Heath et al., 2006a) that the aggregated calcite flocs would be larger than the non-flocculated spherical glass. Additionally, the relatively small length to width ratio may have contributed to a reduced performance. Hence, it is perhaps not surprising that the weir samples detected elevated particle concentrations for the glass trial. Nevertheless, as the weir samples were over an order of magnitude lower than the feed (with the average weir concentration being ~0.75 g/l against the inlet of 34 g/l) the suspension sedimentation performance was considered satisfactory for the purposes of comparing to CFD predictions.

CFD simulations of concentration profiles for the settling glass dispersions along the clarifier at the last two measurement times are presented in Fig. 4 (results for all times are shown in the ESM, Fig. S5). These represent central plane concentrations from the mesh. It is clear from these colour plots that particle concentration is largely consistent between the last two measurement times, indicating a steady-state equilibrium had been established for the suspension zone, noting however that in these models, the solids are removed from the base of the clarifier, whereas in practice, the bed increases in depth, albeit by a small amount. It is also evident that the profiles show very little variation along the clarifier (at least within the settling section) suggesting that most of the dispersion settles relatively rapidly, although there is a clear upturn in concentration at the very end of the clarifier for the final time-step (highlighted by the brighter green region). It is assumed this instability was caused by a recirculation current forming in the clarifier, commonly observed in

unbaffled clarifiers (Fan et al., 2007; Tarpagkou and Pantokratoras, 2014). This was also evident visually in the clarifier to some degree during the trials, although it was hard to assess whether the recirculation impacted on overall settler performance significantly.

As there was no considerable variation in simulated concentrations profiles along the clarifier, it was decided to take an average profile for the distance covered by the sample positions (i) – (v) (being an absolute distance of 0.75 to 3.75 m from the near end of the settling section of the clarifier) for each time-step and compare results to samples taken at each position. Comparisons showing measured concentrations for positions (i), (ii), (iv) and (v) along with the averaged simulated concentrations versus depth at the final measurement time (+230 min) are shown in Fig. 5 for the glass suspensions. Data for all times are also given in Fig. S5.

The average CFD concentration profile correlates closely to the samples at each of the five length locations (largely appearing to fall between sampled ranges) and demonstrates that the predicted sedimentation behaviour closely matches the experimental system for the glass suspensions, where settling is weakly hindered (due to the relatively low concentrations). This comparison also serves to help validate the industrially applicable modelling framework used, and in particular, that there was sufficient resolution in the computational cells to capture the critical phase changes occurring. While there is a degree of scatter in the experimental data, importantly, there is no significant trending changes from positions (i) – (v). Because of the number of samples required, data from each point is only representative of a single measurement, and thus differences between samples are assumed to be mainly due to statistical variability. Importantly also, there is no evidence of an increase in sampled concentration in the final position closest to the outlet, although, as predicted by the CFD simulation, any such increase would fall beyond the final sample position. The simulated and experimental data are consistent, and show that recirculation does not affect concentration profiles to a considerable degree.

3.2 Comparison between experimental samples and CFD predictions of concentration profiles with flocculated calcite

Averaged feed and weir sample values for the flocculated dispersion trial at the five measurement times are also presented within the ESM Fig. S4 (a) and (b). Similar to the glass trial, feed concentrations were relatively consistent over time. The overall settling performance was much greater for the flocculated calcite, with weir concentrations giving an average of ~0.13 g/l (or ~52 $ppm_{,v}$), i.e. substantially lower than for the glass dispersions. This result is consistent with the calcite flocs being considerably larger in size than the glass, as expected (Heath et al., 2006a).

Indeed, *in situ* FBRM measurements taken during the trial in the mixer zone gave a relatively consistent chord length median of ~80 - 90 μm with little variation throughout the run time (see ESM, Fig. S6). It is noted that this size is above maximum values measured in the batch mixing analysis (Fig. 2 (a)), although this is likely due to differences in shear and mixing efficiency between the stirred tank and inlet pipeline. Nevertheless, it is clear that the 5.3 m lead-in section (from the floc injection point to clarifier inlet) was sufficient to cause high levels of aggregation, given the relatively large measured sizes in the mixing region.

CFD simulations of interpolated concentration profiles for the settling flocculated calcite across the clarifier for the last two measurement times, are shown in Fig. 6. Results for the first three times are given in the ESM, Fig. S7. As with the glass dispersions, these represent central plane concentrations. Unlike the glass dispersions, predicted colour-plots for the flocculated calcite suggest considerable differences in clarifier concentration between measuring times, and indicate that even after four hours of operation, a steady-state equilibrium has not been reached within the suspension zone above the bed. In particular, the final time-step at +240 min predicts a significant increase in particle levels (although jumps in concentration are evident at all times, see Fig. S7). It is also evident that there was more variation in depth profiles along the length of the clarifier. Nonetheless, it was considered that the differences were still small enough that an overall average concentration profile for the length of the clarifier at each time-step would be appropriate to compare to sample data. The average simulated profile for the final time-step is shown in Fig. 7, in comparison to sampled values for horizontal positions (i), (ii), (iv) and (v), with profiles are compared to all experimental samples at all measurement times in the ESM, Fig. S7.

The concentration profiles presented in Fig. 7 show a much poorer correlation between simulation and experimental results for the flocculated calcite, and that the model under-predicts particle concentrations in the clarifier (or is essentially over-predicting particle sedimentation). However, both simulation and experimental results show that clarifier dispersion levels for the calcite systems are much lower than for the glass dispersions (see Fig. 6) which is consistent with the greater separation efficiency of the flocculated calcite (as measured from the lower overflow levels in the weir, presented in Fig. S4).

It is thought that the main cause of the relatively poor comparison between the model predictions and experiment was likely due to difficulties in resolving the complex flows within the initial mixer region, and in particular, uncertainty over the flocculation and breakup rates and variation in the

436 collision efficiency i.e. the fraction of collisions that lead to attachment. Experimental bed sampling
437 suggested an equilibrium consolidated bed formed of 0.2 – 0.3 m in the mixer zone, while
438 simulations indicated that over time a much higher bed (> 0.5 m) was created. These differences
439 could be attributable to a number of causes. Firstly, as discussed in the methodology, the impeller
440 was resolved implicitly using a momentum source, to save computational time, with the limitation
441 that the momentum is applied in the vertical component and does not resolve any swirl. Thus, the
442 shear environment is not resolved in any detail around the mixer, which may have an influence on
443 the floc sizes that pass over the weir. Secondly, the aggregation and breakup model constants and
444 collision efficiency are based on fitting the model at a single shear velocity gradient and average
445 particle size, rather than a measured particle size distribution. Thus, there is some uncertainty over
446 the accuracy of the model constants. Additionally, although ignoring particle re-suspension in the
447 clarifier settling zone (due to low levels of turbulence) may be appropriate, it could be an over
448 simplification in the mixer region. Overall, it was deemed too computationally expensive to
449 explicitly resolve the impeller and too analytically complex to include re-suspension from the bed
450 (indeed, the physics of bed erosion and particle re-suspension for cohesive sediments is relatively
451 poorly understood from a particle-fluid mechanics level (Hunter et al., 2013)). Further, there may
452 have been some variance in simulated particle properties. While it was expected from the original
453 pipeline modelling (Heath et al., 2006b) that the particles would be close to a size of ~120 μm, the
454 *in situ* FBRM in the mixer zone (Fig. S6) measured slightly lower values of 80 - 90 μm as discussed,
455 suggesting some degree of breakup in the mixer zone with lower associated settling rates. Also,
456 whereas the floc fractal dimensions were estimated at 2.5, lower values towards 2 or even below
457 are possible, depending on mechanism and shear (Li et al., 2006; Maggi et al., 2007) resulting in
458 lower-density aggregates and corresponding slower settling.
459
460 The sampled data itself in Fig. 7 presents two further important trends. Firstly, there were no
461 samples gained at the lowest level, closest to the base (depth 7) for any of the horizontal positions
462 because these lay below the level of the consolidated bed, unlike the simulation, which contained
463 only a small < 3 cm bed (see Fig. 6). The discrepancy is attributed to the likely over-prediction of
464 the consolidated bed volume fraction, taken at 0.3 in the model. Although reasonable for deep
465 thickener beds, similar flocculated calcite has shown significant variation in particle concentration,
466 depending on depth (Benn et al., 2018). In fact, some samples from the settled bed were taken
467 across the clarifier, and showed that measured volume fractions were only in the range of 0.1 – 0.2,
468 and thus clearly below the value used in the model. A future improvement to the simulation would
469 be to extend the settling model to include the effect of solids consolidation and compression in the

bed, thus avoiding the need to set a uniform bed concentration of the solids. However, such a process would also require more detailed measurements in order to fully characterise the consolidation behaviour.

Additionally, it is evident from samples in Fig. 6 that there is a clear trend of increasing particle concentrations with length along the clarifier (horizontal positions (i) – (v)). This development within the downstream end of the clarifier may appear counterintuitive, but again is indicative of a strong recirculation current, which in the case of the flocculated calcite appears to be re-mixing or mobilising particles to a greater degree than in the glass trials. To highlight this fluid movement, velocity vector profiles from the CFD simulation were generated (from the clarifier central plane) with an example from +180 mins presented in Fig. 8, where it is evident that a strong recirculation current does exist. Nevertheless, given the consistent performance of the clarifier from the low weir concentrations, this recirculation did not appear to impact on overall clarifier performance to a large degree.

3.3 Analysis of the acoustic backscatter response and comparison to sampled concentrations

The acoustic backscatter strength from the probe array was analysed via two different methods to calculate particle concentration in the flocculated-calcite trial. Given in Fig. 9 are examples of the raw backscatter profiles (plotted on a dB scale) versus distance from each of the transducers, where data from the lowermost four probes (channel numbers 7 – 4) are shown for distance locations (i), (ii) and (iii) at the final measurement time of +230 mins. There are several key trends observed in this raw data. The lowest transducers at all horizontal positions show an extremely rapid decay in signal with distance from the transducers, indicative of them being submerged within the consolidated bed (and consistent with sampling data in Fig. 6). Indeed, the bed interface is actually observable from the peak in the response for transducer 6 (second from bottom) at all locations. While the probes were placed at an angle of 20^{o} to the vertical, this angle was low enough to still receive a strong scattering vector from the bed surface. For the upper two probes displayed in the figure (numbers 5 and 4, at all distances) the backscatter strength decays in a weak logarithmic fashion, suggestive of a low concentration dispersion (Hunter et al., 2012a).

To estimate concentration from the whole of the trial data, backscatter data from each probe within the 0.05 – 0.25 m depth segment measured by each acoustic transducer was utilised for all clarifier locations and all times (data from probes that were submerged in the consolidated bed or very near the bed were omitted). Initially, the *G*-function approach was used (Rice et al., 2014), which is a

method to quantify acoustic attenuation characteristics. Here, $G = \ln(\Psi r V_{rms})$, where *'V_{rms}'* is the root mean square of the return pulse echo voltage at a particular distance *'r'* from the transducer and *'Ψ'* is the nearfield correction factor, which is estimated using a correlation dependent on transducer face width, distance and frequency, and becomes unity in the acoustic far field (Downing et al., 1995). The *G*-function relationship should give a linear gradient versus distance (as long as particle concentrations within the 0.05 – 0.25 m segment are relatively constant) where d*G*/d*r* (taken from the average gradient) can then be linearly correlated to concentration (Bux et al., 2017; Bux et al., 2019; Rice et al., 2014). Additionally, the backscatter power was measured by integrating the returned backscatter voltage strength over the same profile distance (0.05 – 0.25 m). Measured d*G*/d*r* values and backscatter power values for each probe depth and measurement time (not within the consolidated bed) were correlated to the corresponding sampled particle concentrations and are compared directly in Fig. 10.

The results presented in Fig. 10 indicate that both methods give reasonable linear correlations to concentration, but quantitatively, the backscatter power method led to improved results with a higher R^2 value (of 0.81 in comparison to 0.65 for the *G*-function data). It is expected that the foremost reason for the difference in performance was due to the low concentration of particles in the system. The d*G*/d*r* gradient is essentially a linearised measure of the acoustic signal decay (Bux et al., 2019). Therefore, it would become more accurate at higher concentrations which increasingly attenuate the signal (normally, > 5 g/l (Bux et al., 2017; Bux et al., 2019; Rice et al., 2014)). On the other hand, direct dependency between backscatter strength or power and concentration is only true for relatively dilute dispersions, below regions where significant inter-particle scattering acts to alter the attenuation response (particle levels < ~10 g/l (Hunter et al., 2012a; Simmons et al., 2017)). Given that all sampled concentrations (not within the consolidated bed) were < 8 g/l, it is perhaps not surprising that the backscatter power method gave a closer correlation in this case.

The physical relevance of the d*G*/d*r* values from the *G*-function method are briefly noted. It would be expected that values would tend towards small non-zero negatives (associated with the attenuation of water) at low concentrations (Bux et al., 2019; Thorne and Buckingham, 2004). However, it is clear that values at low particle levels tended instead to small positive gradients. We believe this difference is due to the near-field correction factor not appropriately correlating the particular nearfield pressure profile of the transducers employed, leading to incorrectly modified d*G*/d*r* at greater distances, resulting in these small positive gradients. Similar discrepancies have been reported previously (Rice et al., 2014), but as the correction factor is concentration

538 *independent*, it should only result in a constant off-set, depending on the acoustic-mechanical
539 specifics of the transducers. Therefore, the gradient change of d*G*/d*r* with particle concentration
540 should remain valid and linear, regardless of any off-set values from the nearfield correction factor.
541
542 Due to its reduced variability, the backscatter power correlation was used to conduct a more in-
543 depth comparison to the samples. The seven-channel acoustic data were processed into a colour
544 plot across the five locations along the length of the clarifier for the last three measurement times,
545 as given in Fig. 11 (with change from blue to yellow indicating an increase in backscatter power,
546 correlated to greater concentration). A similar colour-plot was processed for the sample data across
547 the same times and also presented in Fig. 11 (where blue to yellow directly shows an increased
548 concentration, in g/l). As there were only five sample heights, as opposed to the seven acoustic
549 probes, data visualised at depths '2' and '4' from the samples represent a linear interpolation
550 between adjacent points and are not direct measurements.
551
552 It is observed from the colour plots that, qualitatively, sampling and acoustic data compare closely,
553 where regions of greater sampled concentration (colours varying blue to yellow) at the three times
554 largely mirror increases in backscatter power (also coloured blue to yellow). It is noted that the full
555 back-calibration performed in Fig. 10 (b) was not used to convert the backscatter power directly to
556 concentration, to ensure complete independence of measurement for comparison in the colour
557 plots, allowing assessment of whether the performance of the acoustic array was consistent across
558 the clarifier height and length at all times, which appears evident from Fig. 11. Small variations in
559 measured concentrations between samples and the array are to be expected, as it is noted again that
560 samples were from single spatial points with depth, while acoustic data represents averages of 20
561 cm segments. Additionally, there may be some discrepancy from the fact that acoustics and
562 sampling data were laterally off-set by 15 cm (both 7.5 cm either side of the central plane). Data
563 from channel 7 for both samples and acoustics were largely null and void for the three measurement
564 times, as the probes and sampler were both submerged into the consolidated bed. This behaviour
565 is read as a zero backscatter strength with the acoustic analysis (dark blue) and shown as bright
566 yellow in the samples (indicating concentrations >> 8 g/l). Generally however, the strong
567 agreement between techniques highlights the suitability of the acoustic array for continuous online
568 monitoring of suspension separation in a variety of horizontal settler and thickener operations,
569 where sampling is either too logistically difficult, time consuming, or, such as in the case of nuclear
570 waste separation (Johnson et al., 2016), prohibitively hazardous. Additionally, acoustic array
571 monitoring would enable the possibility of real-time operator process control.

572

573 Importantly also, both sampling and acoustic analysis indicate (as does the CFD simulation) that
574 the clarifier is at far from equilibrium conditions in the calcite trial, with an increase in
575 concentrations across the measurement times. Additionally, the colour plots in Fig. 11 highlight
576 the increase in particle levels at the downstream end of the clarifier (locations (iii) – (v)) especially
577 at the final measurement time, consistent with a recirculation current that draws particles up
578 towards the outlet (as evident in the CFD simulations). It is noted that the actual weir position is
579 another metre above the uppermost depth 1, and so largely out of the range of the recirculation.
580 Nevertheless, it is clear that the effects of recirculation are more prominent for the calcite than the
581 glass dispersions. We believe the primary reason may be the fractal structures of the calcite
582 aggregates, leading to complex fluid drag effects that are not present with the spherical glass.
583 Additionally, their relatively low density will mean that any enhancement in turbulence from
584 recirculation may induce mixing to a greater extent than the glass (Gore and Crowe, 1989; Harbottle
585 et al., 2011), despite their larger size and evident greater levels of sedimentation overall in the
586 settling zone.

587

588 # 4 Conclusions

589 The settling performance of a horizontal clarifier was investigated using an innovative ultrasonic
590 research array platform (UARP), allowing multiple depth concentration measurements, and
591 Computational Fluid Dynamics (CFD) simulations. The settler investigated was a 1/3 scale of an
592 operational waste sludge separator, with aim to highlight how both high fidelity *in situ* experimental
593 data and CFD can be combined to improve predictions of semi-continuous solid-liquid separations.
594 Both stable disperse glass dispersions and flocculated calculate were used as sludge simulants, to
595 investigate the behaviour of shear dependent aggregation on sedimentation.

596

597 A population balance solver was used in an open CFD framework (OpenFOAM) to simulate solid-
598 liquid separation, which included hindered settling models, as well as a semi-empirical flocculation
599 and breakup model. Simulations of particle concentration along the clarifier were found to closely
600 correlate to sampled data for glass dispersions, and highlighted that the clarifier had approached an
601 equilibrium state (ignoring accumulation within the bed) within the 230 min operation. With
602 flocculated calcite however, the CFD model appeared to over-predict particle settling, which could
603 be attributable to additional shear breakup of aggregates in the mixing zone and uncertainty over
604 the empirical constants required in the flocculation model. Interestingly, both sampled data and
605 CFD simulations suggested that equilibrium had not been reached for the flocculated calcite trials,

606 highlighting operational complexities from the shear dependent aggregates, representative of many
607 realistic sludge wastes.
608
609 Clarifier settling dynamics for the flocculated calcite trials were probed further, with use of the
610 high resolution UARP, where both the acoustic backscatter power and attenuation were correlated
611 to concentration. Again, it was evident that equilibrium had not been established after +230 min of
612 semi-continuous operation, with particle concentrations continuing to increase. Importantly, the
613 UARP also highlighted evidence of suspension mobilisation by the outlet of the clarifier, due to
614 recirculation currents. Overall, the use of acoustic backscatter was established as a highly effective
615 characterisation technique, suitable for real-time monitoring and control of many large-scale
616 operations, from mineral separation and water treatment to hazardous nuclear waste transfer.
617 Additionally, the ability to gather such high quality experimental data is of value for validation
618 purposes, giving researchers additional tools for the improvement and optimisation of current CFD
619 approaches, which is an area of ongoing research.
620

621 ## Acknowledgments

622 The authors gratefully acknowledge the funding of this work from Innovate UK and Sellafield Ltd.,
623 as part of the *Developing the civil nuclear power supply chain* programme (Grant No: 101433)
624 which contained additional funding from the Nuclear Decommissioning Authority (NDA) and the
625 UK's Engineering and Physical Sciences Research Council (EPSRC). The EPSRC are also thanked
626 for additional funding, as part of the DISTINCTIVE nuclear consortium (EP/L014041/1). Great
627 thanks are given to NSG Environmental Ltd, especially Thomas Hurst and Fraser Hardy, for help
628 in conduction of the large-scale clarifier trials. We also thank Luke Hissitt for research support
629 with the batch sedimentation tests. We would lastly thank the anonymous reviewers for their
630 constructive feedback, which helped improve the paper.
631

632 ## References

633 Antonopoulou, E., Rohmann-Shaw, C.F., Sykes, T.C., Cayre, O.J., Hunter, T.N., Jimack, P.K.,
634 2018. Numerical and experimental analysis of the sedimentation of spherical colloidal
635 suspensions under centrifugal force. Physics of Fluids 30, 030702.
636 Asgharzadeh, H., Firoozabadi, B., Afshin, H., 2011. Experimental investigation of effects of
637 baffle configurations on the performance of a secondary sedimentation tank. Scientia Iranica 18,
638 938-949.

639 Benn, F.A., Fawell, P.D., Halewood, J., Austin, P.J., Costine, A.D., Jones, W.G., Francis, N.S.,
640 Druett, D.C., Lester, D., 2018. Sedimentation and consolidation of different density aggregates
641 formed by polymer-bridging flocculation. Chemical Engineering Science 184, 111-125.

642 Biggs, C.A., Lant, P.A., 2002. Modelling activated sludge flocculation using population balances.
643 Powder Technology 124, 201-211.

644 Bokil, S.D., Bewtra, J.K., 1973. Influence of mechanical blending on aerobic digestion of waste
645 activated sludge. Advances in Water Pollution Research - Proceedings of the Sixth International
646 Conference Held in Jerusalem, 421-428.

647 Bridgeman, J., Jefferson, B., Parsons, S.A., 2010. The development and application of CFD
648 models for water treatment flocculators. Advances in Engineering Software 41, 99-109.

649 Brown, P.P., Lawler, D.F., 2003. Sphere drag and settling velocity revisited. Journal of
650 Environmental Engineering 129, 222-231.

651 Burt, D.J., 2010. Improved design of settling tanks using an extended drift flux model. PhD
652 Thesis, Department of Mechanical Engineering, University of Bristol, UK.

653 Bux, J., Paul, N., Dodds, J.M., Peakall, J., Biggs, S., Hunter, T.N., 2017. In situ characterization
654 of mixing and sedimentation dynamics in an impinging jet ballast tank via acoustic backscatter.
655 AIChE. J. 63, 2618-2629.

656 Bux, J., Peakall, J., Biggs, S., Hunter, T.N., 2015. In situ characterisation of a concentrated
657 colloidal titanium dioxide settling suspension and associated bed development: Application of an
658 acoustic backscatter system. Powder Technol. 284, 530-540.

659 Bux, J., Peakall, J., Rice, H.P., Manga, M.S., Biggs, S., Hunter, T.N., 2019. Measurement and
660 density normalisation of acoustic attenuation and backscattering constants of arbitrary
661 suspensions within the Rayleigh scattering regime. Applied Acoustics 146, 9-22.

662 Concha, F., Segovia, J.P., Vergara, S., Pereira, A., Elorza, E., Leonelli, P., Betancourt, F., 2017.
663 Audit industrial thickeners with new on-line instrumentation. Powder Technology 314, 680-689.

664 Costine, A., Cox, J., Travaglini, S., Lubansky, A., Fawell, P., Misslitz, H., 2018. Variations in the
665 molecular weight response of anionic polyacrylamides under different flocculation conditions.
666 Chemical Engineering Science 176, 127-138.

667 Cowell, D.M.J., Smith, P.R., Freear, S., 2013. Phase-inversion-based selective harmonic
668 elimination (PI-SHE) in multi-level switched-mode tone- and frequency- modulated excitation.
669 IEEE Transactions on Ultrasonics, Ferroelectrics, and Frequency Control 60, 1084-1097.

670 Cowell, D.M.J., Freear, S., Peakall, J., Smith, I., Rice, H.P., Hunter, T.N., Njobuenwu, D.,
671 Fairweather, M., Barnes, M., Randall, G., 2015. Development of a real-time acoustic backscatter
672 system for solids concentration measurement during nuclear waste cleanup, 2015 IEEE
673 International Ultrasonics Symposium (IUS), pp. 1-4.

674 Crittenden, J.C., Rhodes Trussell, R., Hand, D.W., Howe, K.J., Tchobanoglous, G., 2012.
675 MWH's Water Treatment: Principles and Design, third ed. John Wiley & Sons, NJ.

676 Das, S., Bai, H., Wu, C., Kao, J.-H., Barney, B., Kidd, M., Kuettel, M., 2016. Improving the
677 performance of industrial clarifiers using three-dimensional computational fluid dynamics.
678 Engineering Applications of Computational Fluid Mechanics 10, 130-144.

679 De Clercq, B., Lant, P.A., Vanrolleghem, P.A., 2004. Focused beam reflectance technique for in
680 situ particle sizing in wastewater treatment settling tanks. Journal of Chemical Technology &
681 Biotechnology 79, 610-618.

De Clercq, J., Jacobs, F., Kinnear, D.J., Nopens, I., Dierckx, R.A., Defrancq, J., Vanrolleghem, P.A., 2005. Detailed spatio-temporal solids concentration profiling during batch settling of activated sludge using a radiotracer. Water Research 39, 2125-2135.

Derlon, N., Thürlimann, C., Dürrenmatt, D., Villez, K., 2017. Batch settling curve registration via image data modeling. Water Research 114, 327-337.

Downing, A., Thorne, P.D., Vincent, C.E., 1995. Backscattering from a suspension in the near field of a piston transducer. The Journal of the Acoustical Society of America 97, 1614-1620.

Egarr, D.A., Horton, L., Rice, H., Hunter, T., 2016. Development of flocculation models for improving water treatment 10th European Waste Water Management Conference. AquaEnviro, Manchester.

Fan, L., Xu, N., Ke, X., Shi, H., 2007. Numerical simulation of secondary sedimentation tank for urban wastewater. Journal of the Chinese Institute of Chemical Engineers 38, 425-433.

Farrow, J.B., Fawell, P.D., Johnston, R.R.M., Nguyen, T.B., Rudman, M., Simic, K., Swift, J.D., 2000. Recent developments in techniques and methodologies for improving thickener performance. Chemical Engineering Journal 80, 149-155.

Gladman, B.R., Rudman, M., Scales, P.J., 2010. The effect of shear on gravity thickening: Pilot scale modelling. Chemical Engineering Science 65, 4293-4301.

Gore, R.A., Crowe, C.T., 1989. Effect of particle size on modulating turbulent intensity. International Journal of Multiphase Flow 15, 279-285.

Goula, A.M., Kostoglou, M., Karapantsios, T.D., Zouboulis, A.I., 2008. The effect of influent temperature variations in a sedimentation tank for potable water treatment—A computational fluid dynamics study. Water Research 42, 3405-3414.

Guerrero, M., Rüther, N., Szupiany, R., Haun, S., Baranya, S., Latosinski, F., 2016. The acoustic properties of suspended sediment in large rivers: consequences on ADCP methods applicability. Water 8, 13.

Guo, H., Ki, S.J., Oh, S., Kim, Y.M., Wang, S., Kim, J.H., 2017. Numerical simulation of separation process for enhancing fine particle removal in tertiary sedimentation tank mounting adjustable baffle. Chemical Engineering Science 158, 21-29.

Guyonvarch, E., Ramin, E., Kulahci, M., Plósz, B.G., 2015. iCFD: Interpreted Computational Fluid Dynamics – Degeneration of CFD to one-dimensional advection-dispersion models using statistical experimental design – The secondary clarifier. Water Research 83, 396-411.

Harbottle, D., Fairweather, M., Biggs, S., 2011. The minimum transport velocity of colloidal silica suspensions. Chemical Engineering Science 66, 2309-2316.

Heath, A.R., Bahri, P.A., Fawell, P.D., Farrow, J.B., 2006a. Polymer flocculation of calcite: Experimental results from turbulent pipe flow. AIChE Journal 52, 1284-1293.

Heath, A.R., Bahri, P.A., Fawell, P.D., Farrow, J.B., 2006b. Polymer flocculation of calcite: Population balance model. AIChE Journal 52, 1641-1653.

Hunter, T.N., Darlison, L., Peakall, J., Biggs, S., 2012a. Using a multi-frequency acoustic backscatter system as an in situ high concentration dispersion monitor. Chemical Engineering Science 80, 409-418.

Hunter, T.N., Peakall, J., Biggs, S., 2012b. An acoustic backscatter system for in situ concentration profiling of settling flocculated dispersions. Miner. Eng. 27–28, 20-27.

Hunter, T.N., Peakall, J., Unsworth, T.J., Acun, M.H., Keevil, G., Rice, H., Biggs, S., 2013. The influence of system scale on impinging jet sediment erosion: Observed using novel and standard measurement techniques. Chemical Engineering Research and Design 91, 722-734.

Hunter, T.N., Usher, S.P., Biggs, S., Scales, P.J., Stickland, A.D., Franks, G.V., 2015. Characterization of bed densification in a laboratory scale thickener, by novel application of an acoustic backscatter system. Procedia Engineering 102, 858 – 866

Jaworski, A.J., Meng, G., 2009. On-line measurement of separation dynamics in primary gas/oil/water separators: Challenges and technical solutions—A review. Journal of Petroleum Science and Engineering 68, 47-59.

Jeldres, R.I., Fawell, P.D., Florio, B.J., 2018. Population balance modelling to describe the particle aggregation process: A review. Powder Technology 326, 190-207.

Johnson, M., Peakall, J., Fairweather, M., Biggs, S., Harbottle, D., Hunter, T.N., 2016. Characterization of multiple hindered settling regimes in aggregated mineral suspensions. Industrial & Engineering Chemistry Research 55, 9983-9993.

Jones, W.P., Launder, B.E., 1972. The prediction of laminarization with a two-equation model of turbulence. International Journal of Heat and Mass Transfer 15, 301-314.

Karpinska, A.M., Bridgeman, J., 2016. CFD-aided modelling of activated sludge systems – A critical review. Water Research 88, 861-879.

Kim, J., Kramer, T.A., 2006. Improved orthokinetic coagulation model for fractal colloids: Aggregation and breakup. Chemical Engineering Science 61, 45-53.

Li, T., Zhu, Z., Wang, D., Yao, C., Tang, H., 2006. Characterization of floc size, strength and structure under various coagulation mechanisms. Powder Technology 168, 104-110.

Maggi, F., Mietta, F., Winterwerp, J.C., 2007. Effect of variable fractal dimension on the floc size distribution of suspended cohesive sediment. Journal of Hydrology 343, 43-55.

Michaels, A.S., Bolger, J.C., 1962. Settling rates and sediment volumes of flocculated kaolin suspensions. Industrial & Engineering Chemistry Fundamentals 1, 24-33.

Mohanarangam, K., Yang, W., Barnard, K.R., Kelly, N.J., Robinson, D.J., 2013. Flow mapping of full scale solvent extraction settlers using pulsed Doppler UVP technique. Chemical Engineering Science 104, 925-933.

Peña, R., Burcham, C.L., Jarmer, D.J., Ramkrishna, D., Nagy, Z.K., 2017. Modeling and optimization of spherical agglomeration in suspension through a coupled population balance model. Chemical Engineering Science 167, 66-77.

Ramin, E., Wágner, D.S., Yde, L., Binning, P.J., Rasmussen, M.R., Mikkelsen, P.S., Plósz, B.G., 2014. A new settling velocity model to describe secondary sedimentation. Water Research 66, 447-458.

Razmi, A.M., Bakhtyar, R., Firoozabadi, B., Barry, D.A., 2013. Experiments and numerical modeling of baffle configuration effects on the performance of sedimentation tanks. Canadian Journal of Civil Engineering 40, 140-150.

Rice, H.P., Fairweather, M., Hunter, T.N., Mahmoud, B., Biggs, S., Peakall, J., 2014. Measuring particle concentration in multiphase pipe flow using acoustic backscatter: Generalization of the dual-frequency inversion method. J. Acoust. Soc. Am. 136, 156-169.

Rice, H.P., Fairweather, M., Peakall, J., Hunter, T.N., Mahmoud, B., Biggs, S.R., 2015. Measurement of particle concentration in horizontal, multiphase pipe flow using acoustic

methods: Limiting concentration and the effect of attenuation. Chemical Engineering Science 126, 745-758.

Salem, A.I., Okoth, G., Thöming, J., 2011. An approach to improve the separation of solid–liquid suspensions in inclined plate settlers: CFD simulation and experimental validation. Water Research 45, 3541-3549.

Schewerda, J., Forster, G., Heinrichmeier, J., 2013. Novel method for sludge blanket measurements. Water Science and Technology 69, 775-782.

Shahrokhi, M., Rostami, F., Md Said, M.A., Sabbagh Yazdi, S.R., Syafalni, 2012. The effect of number of baffles on the improvement efficiency of primary sedimentation tanks. Applied Mathematical Modelling 36, 3725-3735.

Simmons, S.M., Parsons, D.R., Best, J.L., Oberg, K.A., Czuba, J.A., Keevil, G.M., 2017. An evaluation of the use of a multibeam echo-sounder for observations of suspended sediment. Applied Acoustics 126, 81-90.

Smith, P.R., Cowell, D.M.J., Raiton, B., Ky, C.V., Freear, S., 2012. Ultrasound array transmitter architecture with high timing resolution using embedded phase-locked loops. Ultrasonics, Ferroelectrics and Frequency Control, IEEE Transactions on 59, 40-49.

Spehar, R., Kiviti-Manor, A., Fawell, P., Usher, S.P., Rudman, M., Scales, P.J., 2015. Aggregate densification in the thickening of flocculated suspensions in an un-networked bed. Chemical Engineering Science 122, 585-595.

Stamou, A.I., Adams, E.W., Rodi, W., 1989. Numerical modeling of flow and settling in primary rectangular clarifiers. Journal of Hydraulic Research 27, 665-682.

Stener, J.F., Carlson, J.E., Sand, A., Pålsson, B.I., 2016. Monitoring mineral slurry flow using pulse-echo ultrasound. Flow Meas. Instrum. 50, 135-146.

Tarpagkou, R., Pantokratoras, A., 2014. The influence of lamellar settler in sedimentation tanks for potable water treatment — A computational fluid dynamic study. Powder Technology 268, 139-149.

Tarud, F., Aybar, M., Pizarro, G., Cienfuegos, R., Pastén, P., 2010. Integrating fluorescent dye flow-curve testing and acoustic Doppler velocimetry profiling for in situ hydraulic evaluation and improvement of clarifier performance. Water Environment Research 82, 675-685.

Thorne, P.D., Buckingham, M.J., 2004. Measurements of scattering by suspensions of irregularly shaped sand particles and comparison with a single parameter modified sphere model. The Journal of the Acoustical Society of America 116, 2876-2889.

Thorne, P.D., Hanes, D.M., 2002. A review of acoustic measurement of small-scale sediment processes. Cont. Shelf Res. 22, 603-632.

Thorne, P.D., Hurther, D., 2014. An overview on the use of backscattered sound for measuring suspended particle size and concentration profiles in non-cohesive inorganic sediment transport studies. Continental Shelf Research 73, 97-118.

Torfs, E., Balemans, S., Locatelli, F., Diehl, S., Bürger, R., Laurent, J., François, P., Nopens, I., 2017. On constitutive functions for hindered settling velocity in 1-D settler models: Selection of appropriate model structure. Water Research 110, 38-47.

Vajihinejad, V., Soares, J.B.P., 2018. Monitoring polymer flocculation in oil sands tailings: A population balance model approach. Chemical Engineering Journal 346, 447-457.

van Deventer, B.B.G., Usher, S.P., Kumar, A., Rudman, M., Scales, P.J., 2011. Aggregate densification and batch settling. Chemical Engineering Journal 171, 141-151.

Vanrolleghem, P.A., De Clercq, J., De Clercq, B., Devisscher, M., Kinnear, D.J., Nopens, I., 2006. New measurement techniques for secondary settlers: A review. Water Science & Technology 53, 419-429.

Vanrolleghem, P.A., Lee, D.S., 2003. On-line monitoring equipment for wastewater treatment processes: state of the art. Water Science & Technology 47, 1-34.

Wilson, G.W., Hay, A.E., 2015. Acoustic backscatter inversion for suspended sediment concentration and size: A new approach using statistical inverse theory. Continental Shelf Research 106, 130-139.

Xu, G., Yin, F., Xu, Y., Yu, H.-Q., 2017. A force-based mechanistic model for describing activated sludge settling process. Water Research 127, 118-126.

Zhang, P., Tang, Z., Lv, F., Yang, K., 2019. Numerical and experimental investigation of guided wave propergation in a multi-wire cable. Applied Sciences 9, 1028.

Zhang, Y., Grassia, P., Martin, A., Usher, S.P., Scales, P.J., 2015a. Designing thickeners by matching hindered settling and gelled suspension zones in the presence of aggregate densification. Chemical Engineering Science 134, 297-307.

Zhang, Y., Grassia, P., Martin, A., Usher, S.P., Scales, P.J., 2015b. Mathematical modelling of batch sedimentation subject to slow aggregate densification. Chemical Engineering Science 128, 54-63.

FIGURES

Graphical Abstract

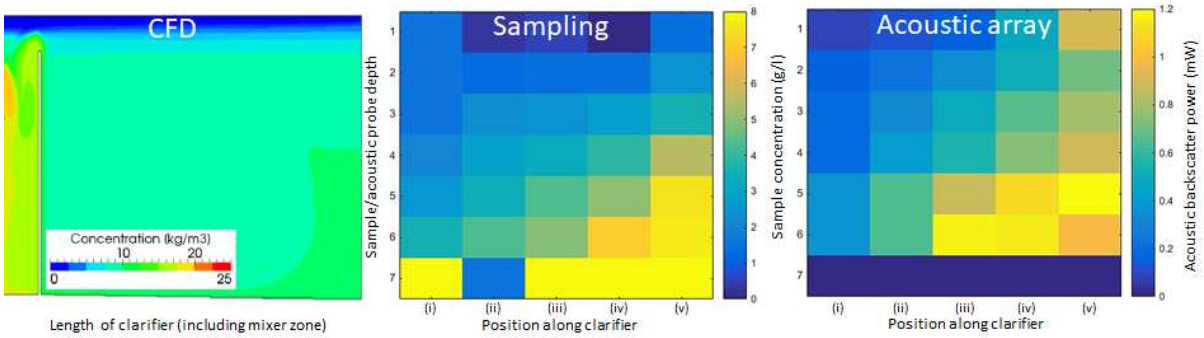

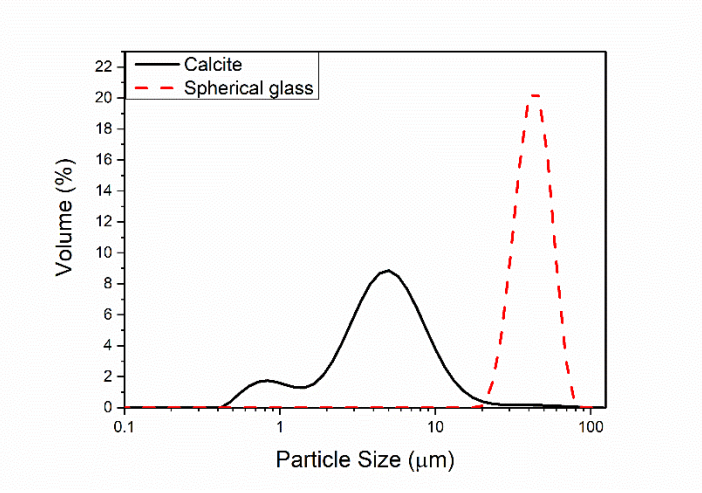

Figure 1: Particle size distributions, measured by laser diffraction, for the unflocculated calcite and spherical glass dispersions. Represented are continuous distributions for bin sizes +/- 6.25% of the floating particle median values.

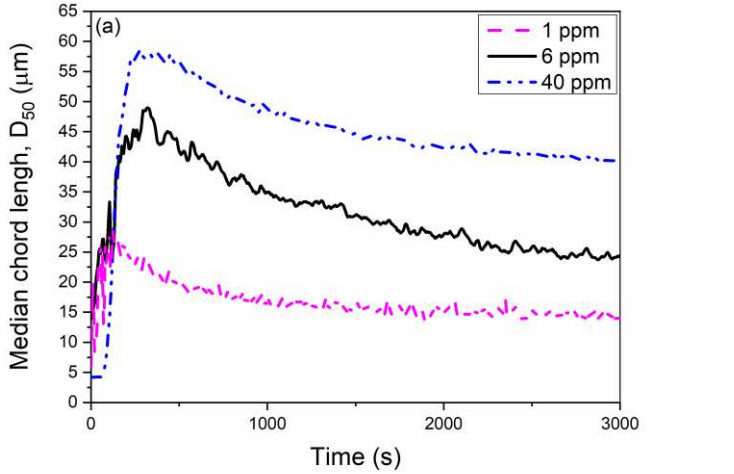

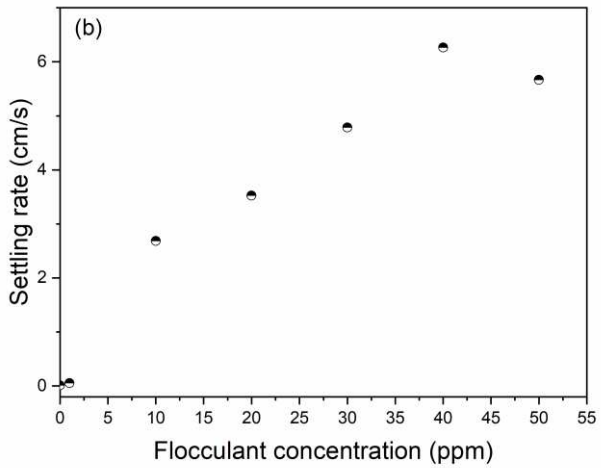

Figure 2: Measured median chord lengths over time, for calcite flocculated with various concentrations of anionic flocculant (a), and average cylinder settling rates for flocculated calcite versus polymer dose (b).

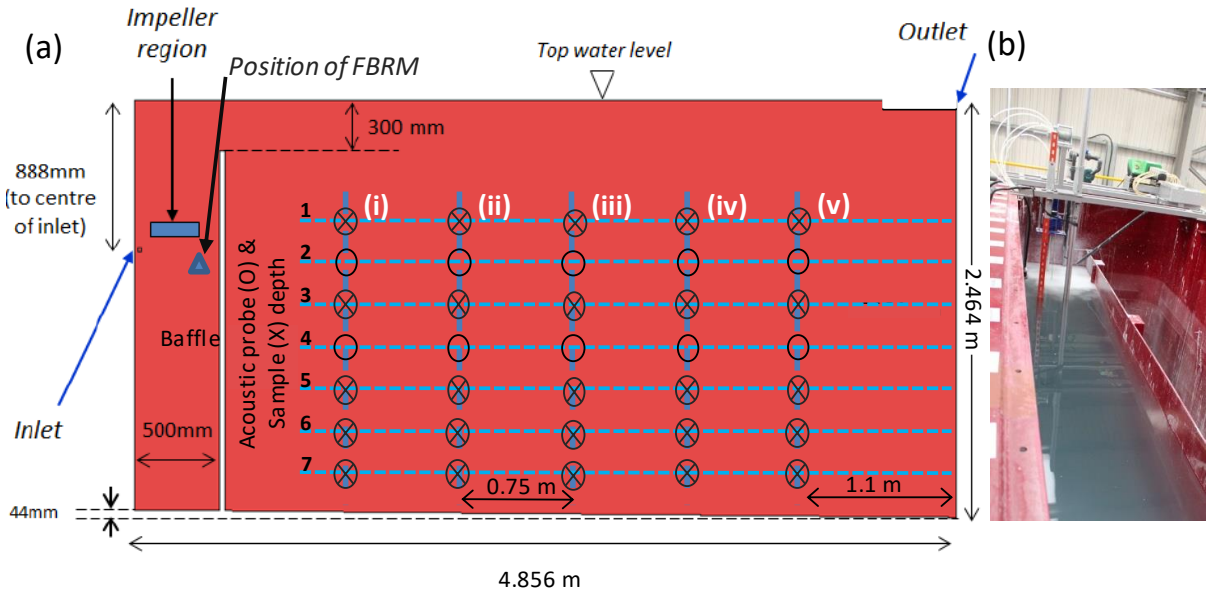

Figure 3: Schematic of settler tank, indicating depths and length positions of taken acoustic and sample data (a), and image of tank with measurement arrays (b).

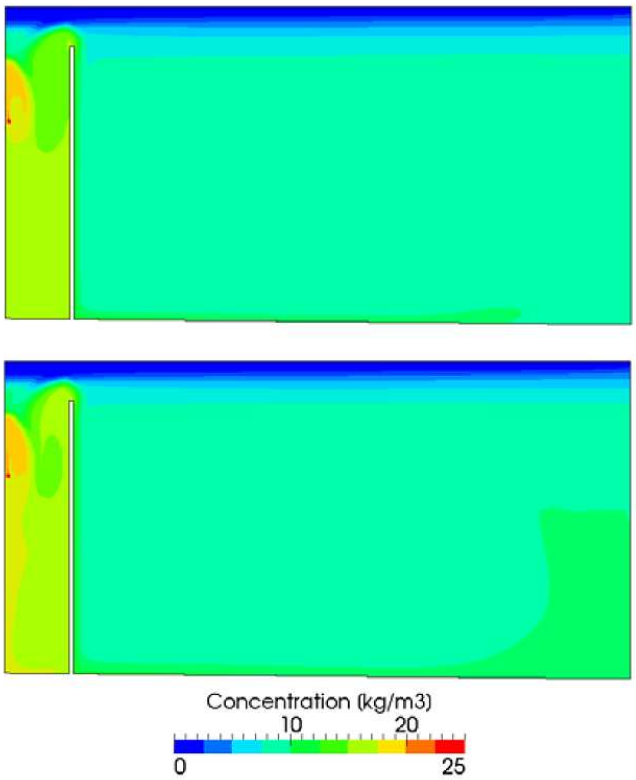

Figure 4: CFD simulation of the non-flocculated glass concentration across the clarifier, for times +180 min (upper) and +230 min (lower). Shown is entire clarifier area (4.856 x 2.464 m^2) at the depth central plane.

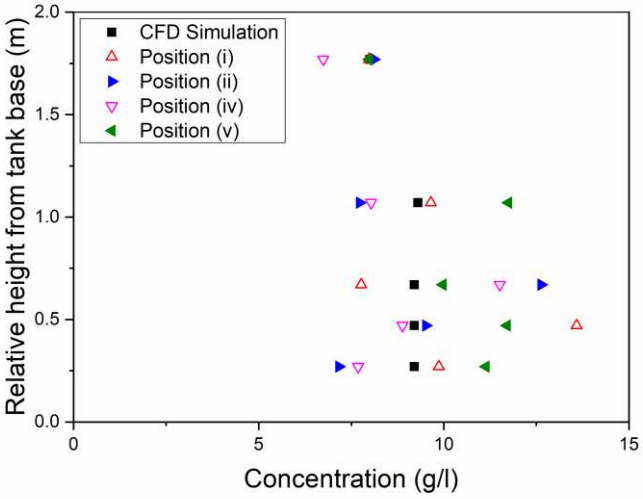

858

859 **Figure 5: Analysis of the average simulated non-flocculated glass dispersion**
860 **concentration at five depths, in comparison to extracted samples across the**
861 **clarifier, at four positions.**

862

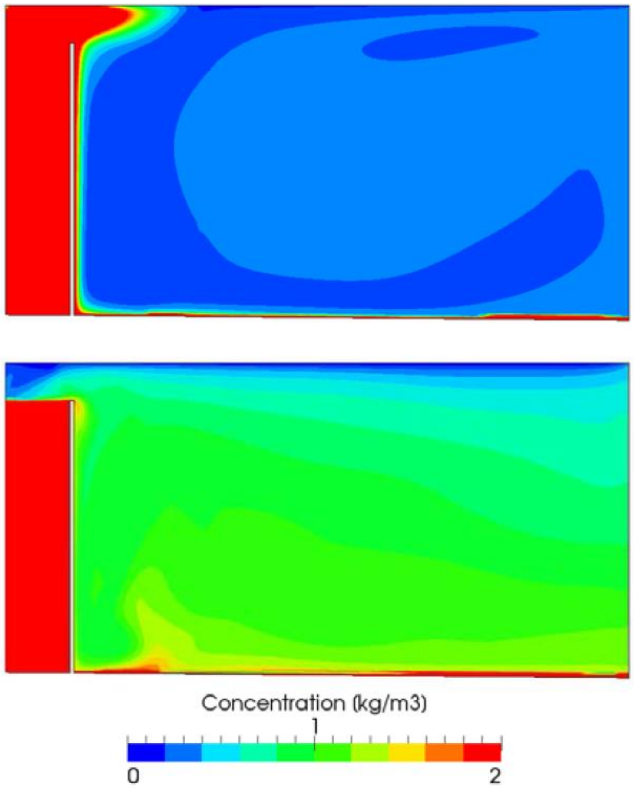

863

864 **Figure 6: CFD simulation of the flocculated calcite concentrations across the**
865 **clarifier, for times +180 min (upper) and +230 min (lower). Shown is entire clarifier**
866 **area (4.856 x 2.464 m^2) at the depth central plane.**

867

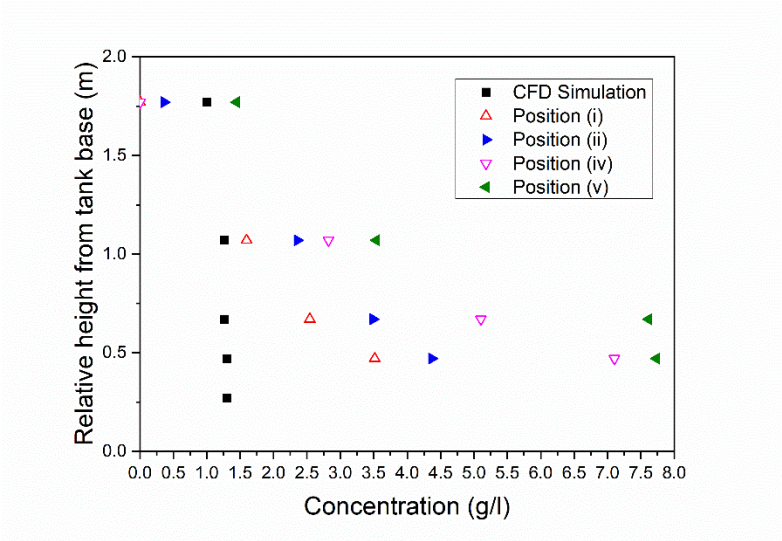

Figure 7: Analysis of the average simulated flocculated calcite concentrations at five depths, in comparison to extracted samples across the clarifier, at four positions.

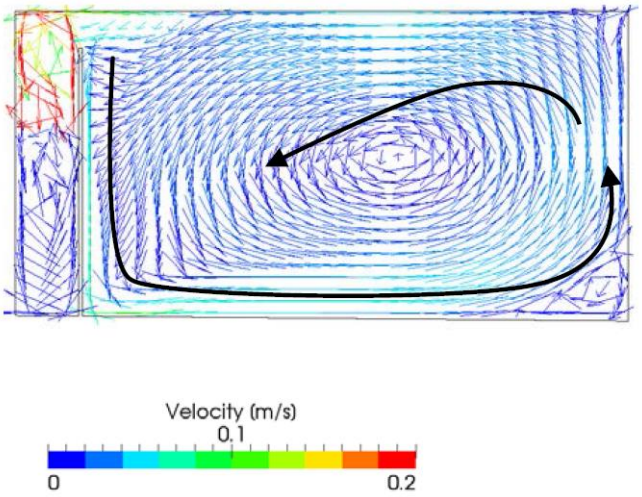

Figure 8: Simulated two-dimensional velocity vector map of the clarifier at time +180 min for the flocculated calcite system. Shown is entire clarifier area (4.856 x 2.464 m^2) at the depth central plane.

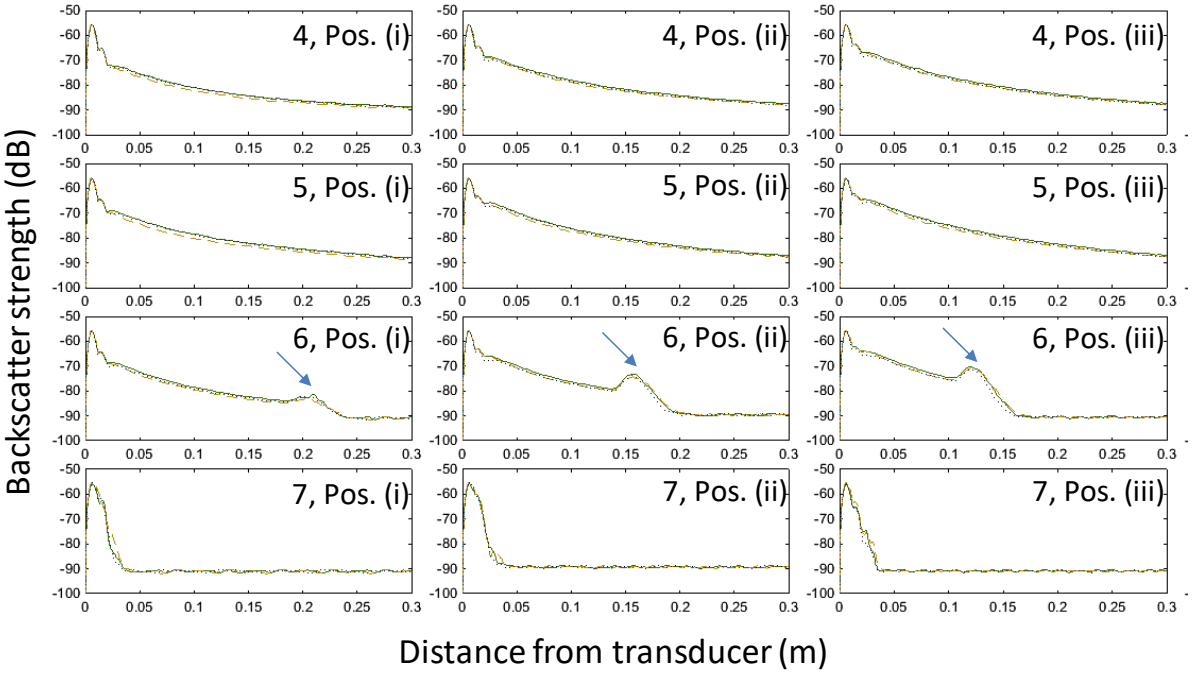

Figure 9: Average acoustic backscatter strength (in db) versus distance from individual transducers at time +230 min. Given are returns for the lowermost four depths (channels 4 – 7) and the first three length positions, (i) – (iii). Annotated arrows indicate backscatter peak from the consolidated sediment bed. Three 1 minute profile averages are shown in all cases.

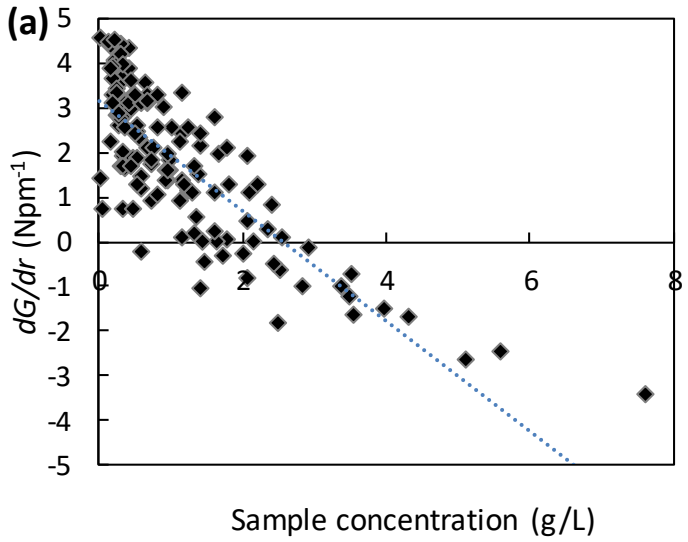

887

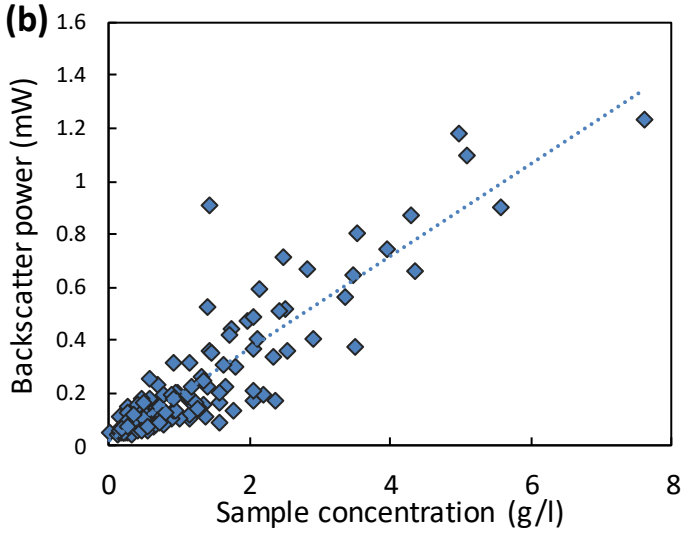

888

889 **Figure 10: Change in acoustic *G*-function/distance gradient (d*G*/d*r*) (a) and**
890 **backscatter power (b) versus measured sample concentrations. Data collated**
891 **from the flocculated calcite trial at all depths and distance positions at all times.**
892 **Points within the consolidated bed were ignored.**

893

894

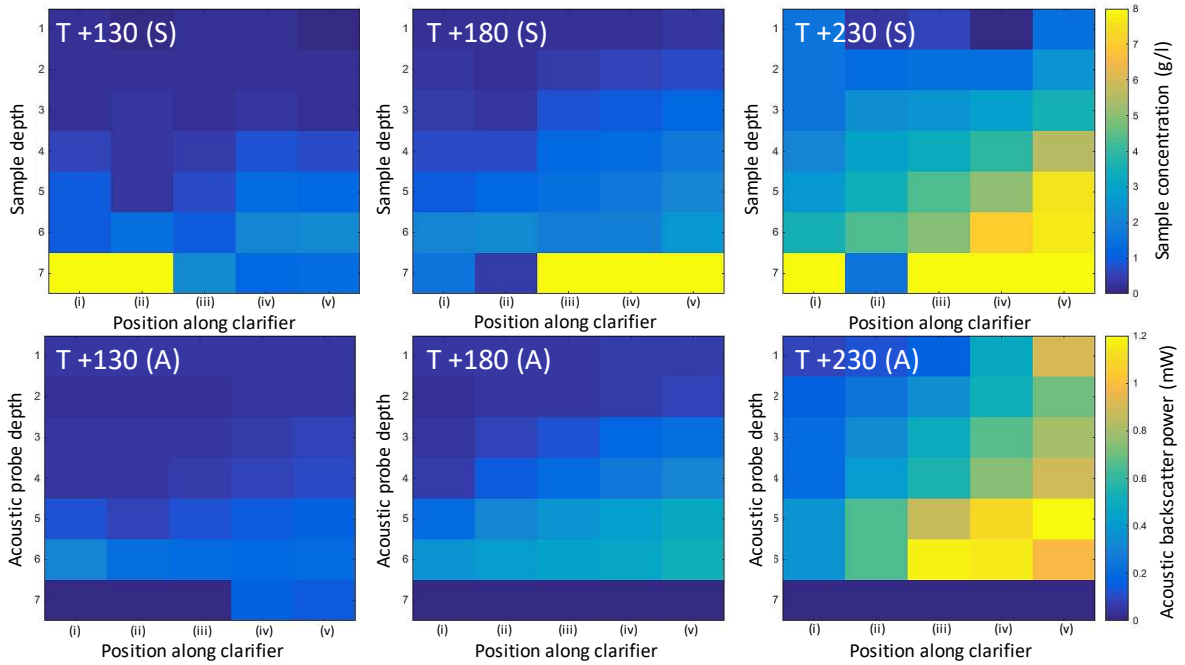

895

896 **Figure 11: (Top) Interpolated colour plot of flocculated calcite particle**
897 **concentrations (in g/l) for sample heights (S) 1 – 7 across all length positions (i) –**
898 **(v). (Bottom) Interpolated colour plot of acoustic backscatter power (in mW) for**
899 **the acoustic channel heights (A) 1 – 7 and the same length positions. Three times**
900 **from commencement of trial (times +130, +180, +230 min) are given for both.**

901